Applied Mathematical Modelling 57 (2018) 206–225

Contents lists available at ScienceDirect

Applied Mathematical Modelling

journal homepage: www.elsevier.com/locate/apm

Comparison of novel variable area convergent-divergent nozzle performances obtained by analytic, computational and experimental methods

Andrija Petrovic[a,*], Jelena Svorcan[b], Aleksandar Pejcev[c], Darko Radenkovic[d], Aleksandar Petrovic[a]

[a] University of Belgrade, Faculty of Mechanical Engineering, Department of Process engineering, Kraljice Marije 16, 11000 Belgrade, Serbia
[b] University of Belgrade, Faculty of Mechanical Engineering, Department of Aerospace engineering, Kraljice Marije 16, 11000 Belgrade, Serbia
[c] University of Belgrade, Faculty of Mechanical Engineering, Department of Mathematics, Kraljice Marije 16, 11000 Belgrade, Serbia
[d] University of Belgrade, Faculty of Mechanical Engineering, Department of Fluid mechanics, Kraljice Marije 16, 11000 Belgrade, Serbia

ARTICLE INFO

Article history:
Received 30 March 2017
Revised 20 December 2017
Accepted 8 January 2018

Keywords:
Variable area nozzle
Ejector
Numerical modeling
Experimental study
Convergent-divergent nozzle

ABSTRACT

Different applications of a variable area convergent-divergent nozzle are found in various parts of the industry. This paper presents the development of a new design methodology for a variable area convergent-divergent nozzle, to maintain constant nozzle area ratio for different values of mass flow rates. The validation of the presented model was carried out on an example supersonic ejector using experimental, numerical and analytical data. Analytical (one dimensional) and computational fluid dynamics models showed satisfactory prediction performance in comparison with the experiment. The average entrainment ratio error was between 10% and 7%, respectively. Results confirmed that the velocity of the primary fluid at the nozzle outlet is in accordance with the one dimensional analysis. Although disturbances (strong and weak shock waves) are visible, their effects are negligible. Also, supersonic ejector performances are presented through relations between entrainment ratio, outlet pressure and spindle position. Disadvantages of variable area nozzle utilization in ejector applications are emphasized.

1. Introduction

Modern technological efforts are primarily influenced by sustainability, concerning environmental problems and energy savings. Utilization of waste and low-grade thermal energy has been an area of interest for researchers and scientists over many years [1], with many examples in the literature (e.g. [2,3]). Specific topics connected with the combustion of very dangerous, explosive, toxic or low caloric value waste gasses have been studied recently (Zhou et al. [4] and Friesenhan et al. [5]). One of the ways of using such gases is by mixing them with high-pressure gas, to make a mixture which is safer or with higher exergy value. This is commonly achieved using supersonic gas ejectors.

Many different studies concerning the optimization of ejector design for various process fluids have been performed. Huang et al. [6] successfully developed a widely used one dimensional (1-D) model for prediction of supersonic ejector

* Corresponding author.
E-mail address: aapetrovic@mas.bg.ac.rs (A. Petrovic).

https://doi.org/10.1016/j.apm.2018.01.016
0307-904X/

Nomenclature

$\dot{m}$, kg/s	mass flow rate;
A, m^2	cross-section area;
a, m/s	speed of sound;
C_p, J/K	heat capacity at constant pressure;
CR	compression ratio;
D, m	diameter;
ER	entrainment ratio;
K	constant;
k, m^2/s^2	turbulence kinetic energy;
L, m	length;
L_{13}, m	nozzle mixing chamber distance;
M	Mach number;
P, Pa	pressure;
Pr	Prandtl number;
R, J/kgK	gas constant;
R_a, m	radius;
T, K	temperature;
t	turbulence intensity;
u, m/s	velocity component;
X, m	spindle coordinate.

Greek symbols

γ	heat capacity ratio;
Π	pressure ratio;
λ	velocity ratio;
ε	density ratio;
φ	friction factor;
μ, Pas	dynamic viscosity;
κ, W/mK	thermal conductivity;
ρ, kg/m^3	density;
ω, 1/s	specific dissipation rate.

Subscripts

0	total properties;
1	nozzle outlet;
2	mixing chamber inlet;
3	mixing chamber outlet;
c	critical properties;
m	mixed flow;
max	maximum;
min	minimum;
out	ejector (diffuser) outlet;
opt	optimal;
p	primary (motive) flow;
$p1$	primary fluid at nozzle outlet;
s	secondary (entrained) flow;
t	turbulence;
tot	total.

performance at critical mode. Comparison between analytical predictions and experimental data resulted in low entrainment ratio (ER) relative errors. Other studies based on this work made some additional enhancements to the previous model, (Liao [7] and Elbel & Lawrence [8]).

Antonio et al. [9] presented an integral method for design of the optimal value of mixing chamber diameter of a supersonic ejector. It included a thermodynamic model based on the 1-D isentropic flow of perfect gases with the addition of a model of losses. The model was validated with three hundred steam ejectors and showed ER relative errors less than 5%. Computational fluid dynamics (CFD) models of ejector performance for different flow geometries have also been used to validate 1-D models and predict flow performances in complicated geometries (Hemidi et al. [10]). Croquer et al. [11] compared predictions of a thermodynamic model and a CFD model. The dimensions of the ejector determined by the 1-D model

were used in the CFD simulation. The thermodynamic model showed higher ER in choking conditions and slightly different values of the critical and limiting pressure ratio.

One of the biggest problems with predicting flow performance of ejectors by CFD is connected with turbulence modeling (Croquer et al. [12]). There is still no agreement on what kind of model should be used. Besagni and Inzoli [13] compared seven RANS (Reynolds Averaged Navier–Stokes) turbulence models under different wall conditions. The $k-\omega$ SST model showed the best performance with maximum ER relative error equal to about 10%. In addition, the shock wave position was also well predicted. Balabel et al. [14] also showed that the shear-stress transport (SST) $k-\omega$ model exhibits the best overall agreement with the experimental measurement of the static pressure on the upper convergent-divergent nozzle surface.

The main disadvantage of supersonic ejectors is their inability to change the mass flow rate of the primary motive steam while maintaining the entrainment ratio and outlet pressure at a constant value. The first solution to this problem is made by analyzing different geometries of the mixing chamber and nozzle and choosing the one with the best-averaged performances, measured by entrainment ratio (ER) or compression ratio (CR). Thongtip and Aphornratana [15] compared six different nozzles and observed their effects on performance of a refrigeration ejector system. Two of the nozzles had the same throat diameter but different nozzle area ratios, whereas four of them had the same nozzle area ratio, but different throat diameters. It was found that using a bigger nozzle throat diameter while operating at a lower generator temperature generally gives a higher COP (coefficient of performance) for different regimes. However, this problem can be better solved by using a variable convergent-divergent nozzle, where the mass flow rate of the motive steam is changing with a throat diameter of nozzle (Varga et al. [16]).

Li et al. [17,18] experimentally evaluated the influence of a variable area nozzle supersonic ejector on a multi-evaporator refrigeration system. They showed that energy efficiency with a variable area ejector could be improved by 12%. Nozzle spindle position also proved to have a great impact on system performance by lowering power consumption. Furthermore, Dennis et al. [19] provided a way to construct a primary nozzle, with a variable throat and variable outlet diameter, to enhance the operating performance of the solar cooling system. The viscous dissipation effect was analyzed by Lelea and Cioabla [20].

Pereira et al. [21] experimentally verified the advantages of using an ejector with variable area nozzle compared to a fixed ejector geometry in refrigeration technology. The variable area nozzle was assembled from the conical spindle and a fixed cylinder. Also, it was shown that nozzle area ratio and nozzle position can be effectively controlled with the spindle, so the position that is optimal for the COP of the cycle can be found for different condenser pressures. Similar results were obtained by Varga et al. [22], showing that adequate selection of the spindle position achieved thermal COP improvements as high as 35%. However, ejectors with this type of variable area nozzle (conical spindle and fixed cylinder) are unable to preserve values of CR and ER in narrow limits, for constant inlet pressures of primary and secondary fluids, while varying the mass flow rate of the primary fluid. This behavior is the consequence of huge total pressure drop which exists due to shockwaves that occur in this type of variable area nozzle.

In this paper, a novel approach for the design of variable area convergent-divergent nozzle is developed to ovecome the above limitation. The nozzle formed from the specially designed spindle with complex geometrical shape and a fixed cylinder has the objective to hold constant nozzle area ratio for different spindle positions. This has the effect of constraining the CR and ER values to an narrow range. Mach number and momentum of primary flow at the nozzle outlet remain unchanged while varying mass flow rates for constant values of pressures at the nozzle inlet and outlet. The influence of shockwaves on primary fluid total pressure drop in this variable area nozzle has a small effect. The performance of the new variable area nozzle design is evaluated experimentally in industrial application for a supersonic gas ejector. Additionally, experimental results were compared with the data obtained by CFD and 1-D models and the advantages of the supersonic ejector with the novel variable area nozzle are presented.

2. A novel method for design of variable area convergent-divergent nozzle

A convergent-divergent nozzle (or De Laval nozzle) is a type of axisymmetric, hourglass shape nozzle that is used to accelerate gas under pressure to a supersonic speed, by converting pressure and internal energy into kinetic energy of fluid flow. The steady flow of the gas through a convergent-divergent nozzle can be modeled by assuming it to be one-dimensional at all sections of the nozzle (quasi-one-dimensional flow) (Oosthuizen & Carscallen [23]). It is also assumed that the flow is isentropic everywhere. The assumption is adequate since the effect of friction and heat transfer is restricted to the thin area near the wall. Hence they can be ignored or accounted for by introducing an empirical constant.

The nozzle area ratio is the ratio of the outlet area of the nozzle and its throat area. The nozzle outlet area should be designed to ensure that the primary flow is expanded in such a way that the static pressure of the expanded flow is as close as possible to the static pressure of the surrounding secondary flow located at the suction chamber. In this way, the irreversibility connected with shockwaves (normal and oblique) as a consequence of the over-expended or under-expended flow is avoided. Possible outcomes of adequate nozzle design are higher values of velocity and momentum achieved at the nozzle outlet.

The effect of a change in the area of the nozzle, ΔA, on the other properties in one-dimensional isentropic fluid flow, is derived using governing equations (mass and energy conservations equations), Eqs. (1) and (2), and the ideal gas equation undergoing the isentropic process, Eq. (3).

$$\rho u A = const \tag{1}$$

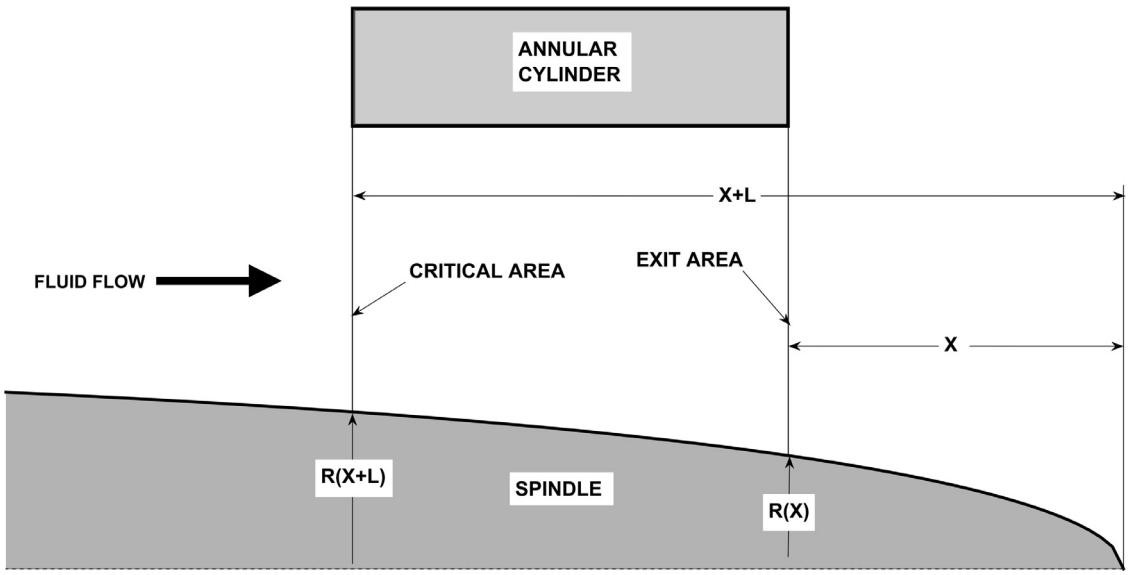

Fig. 1. Variable area convergent-divergent nozzle.

$$u^2 + \frac{2}{\gamma - 1}a^2 = const \tag{2}$$

$$\frac{p}{\rho^{\gamma}} = const \tag{3}$$

The primary flow Mach number at the nozzle outlet and nozzle area ratio can be found from Eqs. (4) and (5), respectively.

$$M_{p1} = \sqrt{\frac{2}{\gamma_p - 1} \cdot \left(\left(\frac{p_{0p}}{p_{p1}} \right)^{\frac{\gamma_p - 1}{\gamma_p}} - 1 \right)} \tag{4}$$

$$\frac{A_{p1}}{A_{pc}} = \frac{1}{M_{p1}} \cdot \left(\frac{2}{\gamma_p + 1} \cdot \left(1 + \frac{\gamma_p - 1}{2} \cdot M_{p1}^2 \right) \right)^{\frac{\gamma_p + 1}{2 \cdot (\gamma_p - 1)}} \tag{5}$$

Mass flow rate of the primary fluid, under choking conditions in nozzle throat, is constant under steady-flow conditions and a function of the heat capacities, total inlet pressure, temperature and throat area. Denoting mass flow rate $\dot{m}_p$, an expression for throat area is:

$$A_{pc} = \frac{\dot{m}_p \cdot \left(\frac{\gamma_p + 1}{2} \right)^{\frac{\gamma_p + 1}{2(\gamma_p - 1)}} \cdot \sqrt{\gamma_p \cdot R_p \cdot T_{0p}}}{p_{0p}} \tag{6}$$

To achieve different mass flow rates through the nozzle, for the same total pressure values, many different variable area nozzle constructions can be used. Most of them are constant area convergent-divergent nozzles with a spindle used as a tool for changing throat area and consequently mass flow rate of the fluid. Despite their simplicity, this kind of variable area nozzle cannot retain constant nozzle area ratio, so huge irreversibility is associated with them.

To solve this problem, a variable area nozzle is formed from the spindle and a fixed cylinder. Additionally, the spindle is designed in such a way that nozzle area ratio does not changing while moving the spindle along its entire operational length. The inlet area between the cylinder and the spindle is the critical area, where choking occurs. To develop a model for constructing the curvature of the spindle the following geometric dimensions are adopted: X presents the axial coordinate starting from the top of the spindle, L is the total cylinder length, D is the diameter of the cylinder and $R_a(X)$ is the radius of the spindle as a function of X. The variable area nozzle model, with geometric characteristics, is presented in Fig. 1.

The purpose of the spindle is to maintain the constant nozzle area ratio, which is presented by Eqs. (7) and (8).

$$\frac{A_{p1}}{A_{pc}} = const = K, K > 1 \tag{7}$$

$$\frac{\left(\frac{D^2}{4} - R_a^2(X)\right)\cdot\pi}{\left(\frac{D^2}{4} - R_a^2(X+L)\right)\cdot\pi} = K \tag{8}$$

The numerator and denominator of Eq. (5) are functions of X, so their simplified form is given by Eqs. (9)–(11).

$$f(X) = \frac{D^2}{4} - R_a^2(X) \tag{9}$$

$$f(X+L) = \frac{D^2}{4} - R_a^2(X+L) \tag{10}$$

$$\frac{f(X)}{f(X+L)} = K \tag{11}$$

This model obviously corresponds to the exponential function that can be presented in the following manner:

$$f(X) = C\cdot s^X \tag{12}$$

where C denotes a constant and s is a function of K.

Moreover, it can be easily proved (including the assumption of continuity of function) that this exponential function is the only one which meets the requirement given by Eq. (11). Constant C can be defined by boundary condition shown in Eq. (10).

$$R_a(0) = 0 \tag{13}$$

By substituting right side of $f(X)$ from Eq. (12) to Eq. (11) and solving Eq. (9), R is found to be:

$$R_a(X) = \sqrt{\frac{D^2}{4} - C\cdot K^{\frac{-X}{L}}} \tag{14}$$

$$C = \frac{D^2}{4} \tag{15}$$

This yields the final expression for the radius of the spindle for different values of X.

$$R_a(X) = \frac{D}{2}\cdot\sqrt{1 - K^{\frac{-X}{L}}} \tag{16}$$

Additionally, the radius of the spindle can be expressed as a function of Mach number at the nozzle outlet and pressure ratio, shown in Eqs. (17) and (18), respectively.

$$R_a(X) = \frac{D}{2}\cdot\sqrt{1 - \left(\frac{1}{M_{p1}}\cdot\left(\frac{2}{\gamma_p+1}\cdot\left(1 + \frac{\gamma_p - 1}{2}\cdot M_{p1}^2\right)\right)^{\frac{\gamma_p+1}{2\cdot(\gamma_p-1)}}\right)^{\frac{-X}{L}}} \tag{17}$$

$$R_a(X) = \frac{D}{2}\cdot\sqrt{1 - \left(\frac{\left(\frac{2}{\gamma_p+1}\right)^{\frac{\gamma_p+1}{2(\gamma_p-1)}}\left(\frac{\gamma_p-1}{2}\right)^{\frac{1}{2}}}{\left[\left(\frac{p_{p1}}{p_{0p}}\right)^{\frac{2}{\gamma_p}} - \left(\frac{p_{p1}}{p_{0p}}\right)^{\frac{\gamma_p+1}{\gamma_p}}\right]^{\frac{1}{2}}}\right)^{\frac{-X}{L}}} \tag{18}$$

If the maximum and minimum mass flow rates through nozzle are given, length X is expressed for both values of mass flow rates by Eqs. (8) and (16), therefore, the total usable length of spindle equals:

$$L_{tot} = X_{\max} - X_{\min} + L \tag{19}$$

In the remainder of this paper, the ejector with variable area nozzle is going to be experimentally, numerically and analytically studied, to confirm advantages of previously presented design methodology.

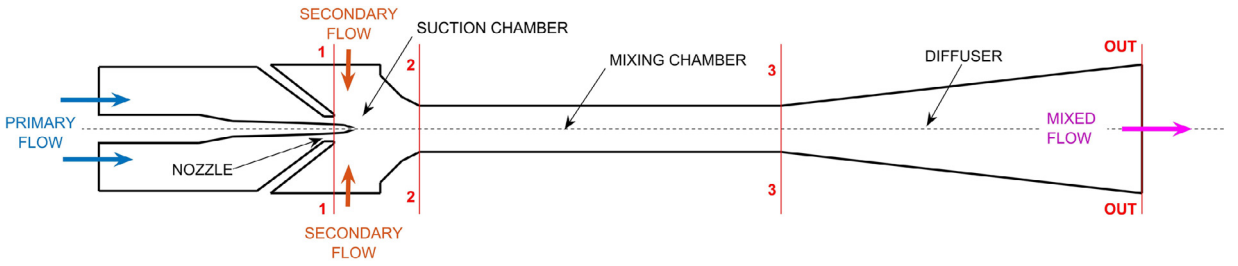

Fig. 2. Geometrical model of supersonic gas ejector with variable nozzle.

3. Supersonic ejector 1-D theoretical analysis

Supersonic jet ejector is a device that uses pressure energy of the primary (motive) fluid, injected into a zone of low pressure, through convergent-divergent nozzle where transformation of pressure to kinetic energy occurs, to suck in and entrain secondary (entrained), low pressure fluid, and to compress the mixed flow to get the desired value of the outlet pressure. The 1-D theoretical analysis of ejector system has to evaluate flow parameters of primary, secondary flow and mixture along the axis by using conservation of mass, momentum, and energy with compressible flow assumptions. Geometrical model and main flow sections of supersonic gas ejector with variable area nozzle are presented in Fig. 2.

The high-pressure primary stream is accelerated through the convergent-divergent nozzle. The primary flow is choked at the throat of the nozzle, thus at the nozzle outlet flow speed is higher than the speed of sound. The supersonic primary fluid flows out into the suction chamber where momentum transfer between primary and secondary fluid occurs. The secondary stream is mixed with the primary flow in the mixing chamber, where oblique and normal shock waves are created and decelerate mixture from supersonic to subsonic speeds, (Kong & Kim [24] and Bouhanguel et al. [25]). Two important characteristics for describing the overall performance of ejectors are entrainment ratio (ER) and compression ratio (CR).

$$ER = \frac{\dot{m}_s}{\dot{m}_p} \tag{20}$$

$$CR = \frac{p_{out}}{p_s} \tag{21}$$

1-D model for prediction of ejector flow performances is used for design and performance evaluation of supersonic variable area ejector. This model proved to be very accurate, in comparison with experimentally measured data, for low values of CR. The model assumes that mixing between different components is ideal, flow is steady and adiabatic, the inlet and outlet velocities of the working fluids in the ejector are neglected. In the present study, a simplified derivation of the ejector performance equation is shown below, more details about this model can be found in Sokolov et al. [26].

The conservation of mass, momentum, and energy can be expressed in the following form:

$$\dot{m}_m = \dot{m}_p + \dot{m}_s = \dot{m}_p \cdot (1 + ER) \tag{22}$$

$$\varphi_2 \cdot \left(\dot{m}_p \cdot u_{p2} + \dot{m}_s \cdot u_{s2}\right) - (\dot{m}_p + \dot{m}_s) \cdot u_3 = \left(p_3 - p_{p2}\right) \cdot A_{p2} + (p_3 - p_{s2}) \cdot A_{s2} \tag{23}$$

$$\dot{m}_p \cdot (c_{pp} \cdot T_p + ER \cdot c_{ps} \cdot T_s) = \dot{m}_p \cdot (1 + ER) \cdot c_{pm} \cdot T_m \tag{24}$$

where ϕ_1, ϕ_2, ϕ_3, ϕ_4 are the empirically obtained coefficients of the nozzle, mixing chamber, diffuser and suction chamber, respectively; $A_3 = A_{s2} + A_{p2}$ is the cross-section area of mixing chamber.

Several assumptions were made concerning pressure of primary and secondary flows in Section 2, Eqs. (24) and (25).

$$p_{p2} = p_{p1} = p_s \tag{25}$$

$$\Pi_{p2} = \frac{p_{p2}}{p_p} = \frac{p_s}{p_p} = \Pi_{ps} \tag{26}$$

The velocities of primary and secondary flows in Section 2 and velocity of mixed flow in Section 3 are:

$$u_{p2} = \varphi_1 \cdot a_{pc} \cdot \lambda_{ps} \tag{27}$$

$$u_{s2} = \varphi_4 \cdot a_{sc} \cdot \lambda_{s2} \tag{28}$$

$$u_3 = \frac{a_{mc}}{\varphi_3} \cdot \lambda_{m3} \tag{29}$$

Table 1
Thermophysical properties and inlet conditions of gases.

	T [°C]	P [Pa]	γ	R [kJ/kgK]
Natural gas	20	251,325	1.304	0.452
Waste gas	40	106,325	1.272	0.383

Table 2
Pressure gauges characteristics.

Fluid	Type	Range [Pa]	Accuracy class	Diameter [mm]	Resolution [Pa]
Natural gas	Bourdon tube	$0–10^6$	1.0	Ø100	$0.2•10^5$
Waste gas	Bourdon tube	$-10^5–3.5•10^5$	1.0	Ø100	$0.1•10^5$
Mixture of gasses	Digital	$0–6•10^5$	0.1	–	10^2

where λ_{ps}, λ_{s2}, λ_{m3} are the ratios of velocities of primary, secondary and mixed flow and their corresponding speeds of sound at critical temperatures, at Sections 1, 2 and 3, respectively.

The speed of sound at the critical temperature of fluid for primary flow is expressed by Eq. (30), and the same expression is valid for secondary and mixed flow.

$$a_{pc} = \sqrt{2 \cdot \frac{\gamma_p}{\gamma_p + 1}} \sqrt{\frac{p_p}{\rho_p}} = \sqrt{2 \cdot \frac{\gamma_p}{\gamma_p + 1}} \sqrt{R_p \cdot T_p} \tag{30}$$

The primary mass flow rate can be presented as

$$\dot{m}_p = \frac{\gamma_p \cdot \Pi_{pc} \cdot p_p \cdot A_{pc}}{a_{pc}} \tag{31}$$

where $\Pi_{pc} = \frac{p_{pc}}{p_p}$ is pressure ratio.

In the case of low CR, it is reasonable to assume that density of the primary and the secondary flow is constant, such that $\gamma_s = \gamma_p = \infty$. Following this assumption and Eqs. (20)–(31) a functional relation between the outlet pressure and other flow parameters of this model, can be presented as

$$\frac{p_{out} - p_s}{p_s} = \gamma_p \cdot \Pi_{pc} \cdot \frac{A_{pc}}{A_3} \cdot \frac{p_p}{p_s} \cdot \left[\varphi_1 \cdot \varphi_2 \cdot \lambda_{ps} + \varepsilon_c \cdot (\varphi_2 \cdot \varphi_4 - 0.5) \cdot \frac{\rho_p}{\rho_m} \cdot \frac{A_{pc}}{A_3 - A_{p1}} \cdot ER^2 - \varepsilon_{pc} \cdot \left(\frac{1}{\varphi_3} - 0.5 \right) \cdot \frac{\rho_{out}}{\rho_p} \cdot \frac{A_{pc}}{A_3} \cdot (1 + ER)^2 \right] \tag{32}$$

where $\varepsilon_{pc} = \frac{\rho_{pc}}{\rho_p}$ is the ratio between critical and total density of the primary fluid.

The optimal cross-section area of the mixing chamber can be obtained from the condition $\frac{\partial p_{out}}{\partial A_3} = 0$.

$$\left(\frac{A_3}{A_{pc}} \right)_{opt} = \frac{2 \cdot \varepsilon_{pc} \cdot \left[\left(\frac{1}{\varphi_3} - 0.5 \right) \cdot \frac{\rho_p}{\rho_m} \cdot (1 + ER)^2 - (\varphi_2 \cdot \varphi_4) \cdot \frac{\rho_p}{\rho_s} \cdot \frac{\frac{A_3}{A_{p1}}}{\frac{A_3}{A_{p1}} - 1} \right]}{\varphi_2 \cdot \varphi_4 \cdot \lambda_{ps}} \tag{33}$$

In addition to the Eq. (33), proper design of mixing chamber diameter requires checking choking conditions.

4. Experimental setup

An experimental ejector with variable area nozzle was tested in industrial installation for the combustion of waste gas, as illustrated in Fig. 3. The experimental ejector test rig is composed of:

(i). The supersonic area ejector with variable area nozzle;
(ii). Pressure regulator for reducing pressure of mixture;
(iii). Spindle position controller;
(iv). Accumulation vessel for waste gas.

Waste gas possesses a large concentration of alkane, highly combustible gas and a small concentration of very explosive gas vinyl-acetate. Because of safety regulations, it is not possible to combust waste gas without reducing the concentration of vinyl-acetate. In addition, waste gas has to be compressed to satisfy requirements for combustion. In order to raise the pressure of the waste gas, high-pressure natural gas (mostly methane), was used as a primary (motive) fluid in the ejector. Thermophysical properties and inlet conditions of waste gas and natural gas are presented in Table 1.

Since the experimental ejector is implemented in an industrial installation, suitable pressure gauges and flow meters must be chosen for proper control of the system. Table 2 shows the characteristics of the pressure gauges used. Measurements of natural and waste gas flow rates were obtained using Vortex flow meters with a digital output containing four

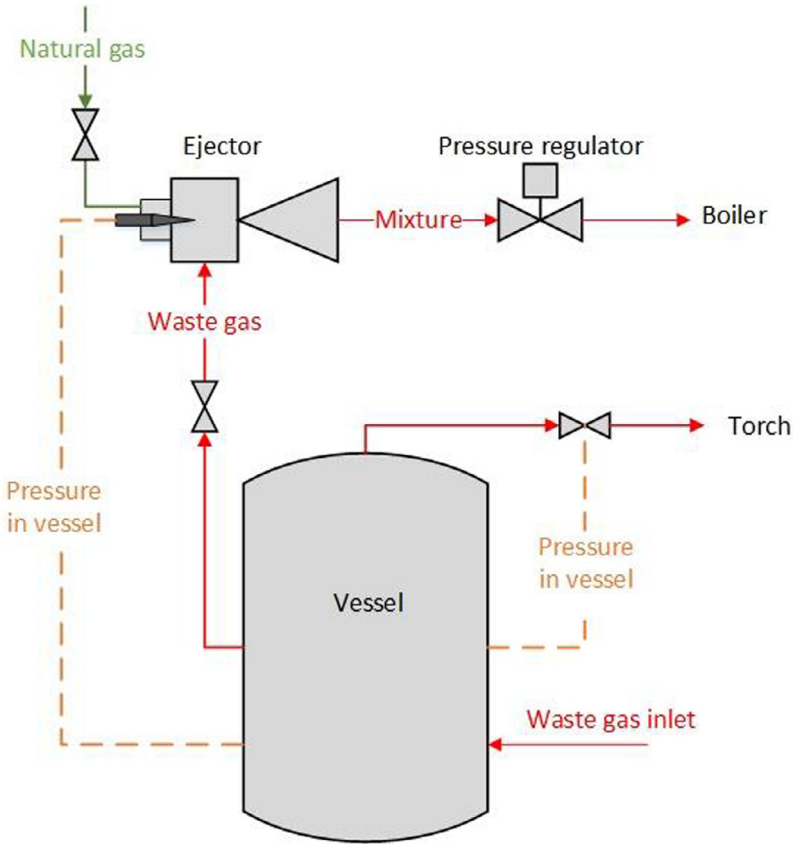

Fig. 3. Installation scheme.

digit decimal number, whereas accuracy class is 1. Two flow meters, with accompanying acquisition and software, were installed.

Depending on the thermal load needs of the final consumer, different mass flow rates of waste gas should be mixed with the natural gas. Furthermore, the ejector has to control ER in limits between 0.58 and 0.67 (mass fraction between 0.35 and 0.4) and outlet gauge pressure in the range between 30 kPa and 50 kPa, to satisfy GHG (green house gases) emission regulations. Maximum and minimum mass flow rates of the waste gas are 350 kg/h and 200 kg/h, respectively. Gauge pressure of the natural gas, primary flow at the ejector inlet, is constant and equal to 150 kPa.

Waste gas is accumulated in the vessel, where gauge pressure varies between 5 kPa and 7 kPa. The pressure in the vessel depends on the waste gas mass flow rate through the ejector and mass flow rate at the inlet of the vessel. Spindle position in the ejector is related to the pressure in the vessel. If the gauge pressure in the vessel is above 6 kPa, the spindle is moved backward so that primary and secondary stream mass flow rates in the ejector are increasing. Moreover, if gauge pressure rises above 7 kPa, a valve that connects the vessel with the torch is opened. In the opposite case, when gauge pressure is below 6 kPa, the spindle is moved forward, and mass flow rates of fluids are decreasing. The internal flow geometry of the ejector is designed according to 1-D analysis (Eq. (33) and previously presented requirements) and constraints, considering choking conditions of secondary flow at the ejector mixing chamber.

The most important dimensions of a supersonic ejector with a variable nozzle are presented in Fig. 4, whereas the photographs of the ejector and variable area nozzle in the installation are shown in Fig. 5a and 5b. The length of the mixing chamber is determined by Eq. (34) (Sokolov et al. [26]), while the diameter is determined in Section 3.

$$L_3 = 7 \cdot d_3 \tag{34}$$

The design of the suction chamber was carried out to reduce friction losses of primary and secondary fluids, such that ER is maximized. The distance between the outlet area of the nozzle and the beginning of the mixing chamber is specified by an empirical correlation shown in [26].

$$L_{13} = \frac{0.37 + ER}{4.4 \cdot a} + \frac{3.4 \cdot d_{1,100\%} \cdot \sqrt{0.083 + 0.76 \cdot ER} - d_3}{\tan(\beta)} \tag{35}$$

where $\beta = 45^o$ is the angle between entrance area of the mixing chamber and ejector axis; $a = 0.07 \div 0.09$ is experimental constant; $d_{ex,100\%}$ is diameter at the outlet area of the nozzle for spindle position 100% opened.

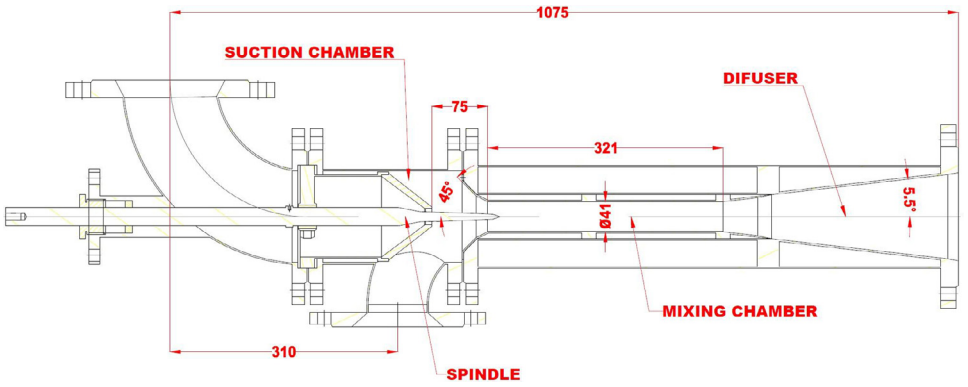

Fig. 4. Supersonic ejector with variable area nozzle.

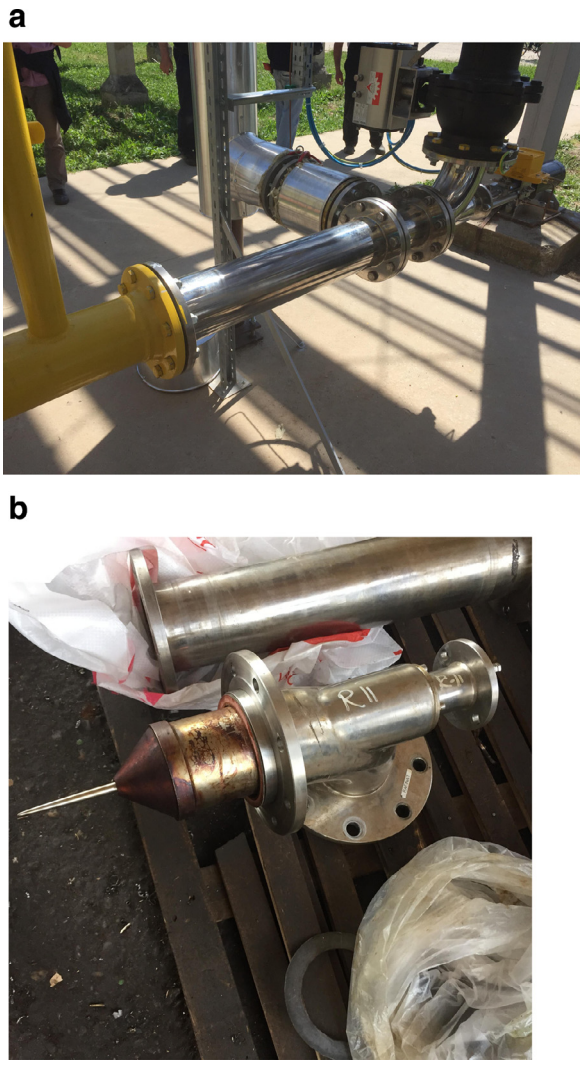

Fig. 5. Supersonic ejector (a) and variable area nozzle (b).

5. CFD model

Numerical simulations were performed in a commercial package ANSYS FLUENT 16.2, with the procedure described in [27]. The flow in the ejector is assumed to be compressible, steady-state and axisymmetric. The total energy equation including viscous dissipation is coupled with the ideal gas law. Although different from reality, for simplicity fluid flow was simulated as single-phase (this is a viable assumption since both gases have similar composition). Assumed fluid characteristics correspond to the natural gas (methane) properties are listed in Section 5.3. Thermal conductivity and viscosity of the gas are constant. Governing equations can be written in the following form:

Continuity:

$$\frac{\partial(\rho u_i)}{\partial x_i} = 0 \tag{36}$$

Momentum:

$$\frac{\partial\left(\rho u_i u_j\right)}{\partial x_j} = -\frac{\partial P}{\partial x_j} + \frac{\partial}{\partial x_j}\left[\mu\left(\frac{\partial u_i}{\partial x_j} + \frac{\partial u_j}{\partial x_i} - \frac{2}{3}\delta_{ij}\frac{\partial u_k}{\partial x_k}\right)\right] + \frac{\partial}{\partial x_j}\left(-\rho\overline{u_i' u_j'}\right) \tag{37}$$

Energy:

$$\frac{\partial}{\partial x_j}\left(u_j(\rho E + P)\right) = \frac{\partial}{\partial x_j}\cdot\left(\left(\lambda_{con} + \frac{C_p\mu_t}{\mathrm{Pr}_t}\right)\cdot\frac{\partial T}{\partial x_j} + u_i\tau_{ij}\right) \tag{38}$$

Ideal gas law

$$p = \rho RT \tag{39}$$

The default value of turbulence Prandtl number Pr_t is equal to 0.85. The momentum equations are closed by a two-equation k-ω SST model that represents a combination of the standard k-ω model near the walls (since it is more accurate and numerically stable in the near wall region) and the k-ε model in the outer layer. It is more reliable than the standard k-ω model particularly for such complex flows involving compressibility, shock and expansion waves, mixing flows, etc. Transport equations are solved for turbulence kinetic energy k and its specific dissipation rate ω. Steady state transport equations of k-ω SST model are shown by Eqs. (40) and (41).

$$\frac{\partial}{\partial x_i}(\rho u_i k) = \frac{\partial}{\partial x_j}\left(\Gamma_k\frac{\partial k}{\partial x_j}\right) + \widetilde{G_k} - Y_k + S_k \tag{40}$$

$$\frac{\partial}{\partial x_i}(\rho u_i \omega) = \frac{\partial}{\partial x_j}\left(\Gamma_k\frac{\partial \omega}{\partial x_j}\right) + G_\omega - Y_\omega + S_\omega + D_\omega \tag{41}$$

where $\widetilde{G_k}$ represents the generation of turbulence kinetic energy due to mean velocity gradients and G_ω is a generation of ω; Y_k and Y_ω are the dissipation of k and ω due to turbulence; Γ_k and Γ_ω represent the effective diffusivity of k and ω, respectively; S_k and S_ω are source terms defined by the user; D_ω is the cross-diffusion term.

5.1. Near wall treatment approach

The near-wall treatment automatically switches from the viscous sublayer formulation to the wall function depending on the distance from the wall. For fine meshes (as used in this study), the viscosity-affected region is entirely resolved all the way to the viscous sublayer. More information on analytical expressions used for the laminar sublayer and wall function approach can be found in [27].

5.2. Boundary conditions

Inlet pressure boundary conditions were imposed at the inlets of primary and secondary flows. Specifically, boundary conditions concerning the values of total and static pressure ($p_p = 251{,}325$ Pa, $p_s = 106{,}325$ Pa), total temperature ($Tp = 20$ °C, $Ts = 40$ °C), flow direction and turbulence quantities (in the form of turbulence intensity $t = 5\%$ and turbulence viscosity ratio $\mu_t/\mu = 10$) were specified. Since turbulence intensity t presents the ratio of the root-mean-square of the velocity fluctuations to the mean flow velocity, it can be used for the computation of the inlet turbulence kinetic energy k. Similarly, the value of specific dissipation rate ω at the inlet can be obtained from k and turbulence viscosity ratio since the latter is directly proportional to the turbulence Reynolds number $\mathrm{Re}_t\,(=k/\omega\nu)$. An outlet pressure boundary condition with a fixed value of static pressure is defined at the ejector outlet. The no-slip condition was applied to all wall surfaces. An outlet pressure boundary condition with a fixed value of static pressure is defined at the ejector outlet. The no-slip condition was applied to all wall surfaces.

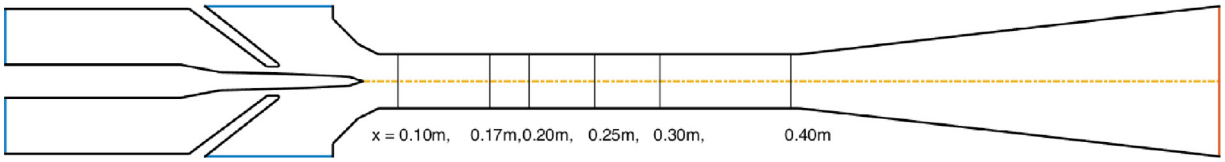

Fig. 6. Computational domain of an arbitrary geometry (spindle at 40%) used in mesh convergence study and six characteristic cross-sections (six reference points are located at the intersection of the axis and cross-section line).

Table 3
Mesh quality.

	M1	M2	M3	M4	M5	M6	Note
Face size [mm]	1.6	1.3	1	0.8	0.6	0.4	In whole domain
Edge size [mm]	0.8	0.65	0.5	0.4	0.3	0.2	In nozzle region
Δy_1 [mm]	0.05	0.02	0.01	0.01	0.01	0.01	First layer thickness
N	13	17	20	20	20	20	Number of layers
Element quality	0.60183	0.57243	0.58837	0.65183	0.71779	0.80505	Ideal 1
Skewness	0.08055	0.07736	0.07396	0.06106	0.06193	0.05284	Ideal 0
Orthogonal quality	0.98097	0.98207	0.98345	0.98777	0.98819	0.99109	Ideal 1
Number of nodes	23,637	36,412	57,758	81,448	127,643	252,175	–
Number of elements	22,934	35,548	56,654	80,053	125,815	249,442	–

5.3. Material properties

Methane properties used in simulations are as follows: specific gas constant $R = 0.518$ kJ/kgK, specific heat ratio $\gamma = 1.307$, molecular viscosity $\mu = 1.087 \bullet 10^{-5}$ Pas, thermal conductivity $\kappa = 0.0332$ W/mK, specific heat $c_p \approx 2200$ J/kgK, molecular Prandtl number $\mathrm{Pr} = 0.72$ (computed from μ, κ and c_p), speed of sound in the undisturbed flow $a = 453$ m/s.

5.4. Discretization criteria

An implicit density-based solver (where the governing equations are solved simultaneously and equations for additional scalars are solved afterwards) was used. Convective fluxes were evaluated by an upwind, flux-difference splitting scheme. Variable gradients were computed by the Least Squares Cell-Based method. Spatial discretizations of flow quantities were second order upwind. The Courant (CFL) number was set to 5 or less. Default values of under-relaxation factors were used except in a few cases when they were slightly reduced.

5.5. Convergence criteria

Several separate conditions were used to define the convergence criteria. Firstly, all computations were performed until scaled residuals fell below 10^{-3}. Secondly, the values of mass flow rates at the inlet and outlet boundaries, and Mach numbers calculated at six different points (Fig. 6), located along the axis in the mixing chamber, had to achieve local convergence. This condition required the relative difference between values in the last five hundred and two consecutive iterations to be less than 0.05% and 0.001%, respectively.

5.6. Mesh quality criteria and independency study

Since several different computational grids had to be created (each corresponding to a different position of the spindle) a grid convergence study was performed in order to assess the set of appropriate mesh properties (e.g. size functions, boundary layer properties) to be used in all subsequent computations. A compromise between accuracy, simplicity, and similarity to real geometry was made. Therefore, all generated meshes are planar, hybrid unstructured with a number of layers forming the near-wall region. However, the comparison of unstructured meshes is not so straightforward, and for that reason, some size parameters are constant for some meshes (Table 3); for example the thickness ratio in the boundary layer is set to 1.2 for all meshes. Tested meshes (corresponding to a single spindle position at 40%) M1-M6 differ in overall cell size (and cell edge size in the nozzle region) and boundary layer definition (number of layers, first layer thickness, dimensionless wall distance y^+). They are enumerated as M1, M2, M3, M4, M5 and M6 according to their refinement.

The quality of the generated meshes can be estimated by several parameters, [27]. Element quality is a global parameter whose values lie in the range [0,1] where 1 indicates a cube or a square while 0 indicates an element of zero or negative volume. Skewness is a highly recognized metric that illustrates how similar an element is to an ideal (equilateral and equiangular) face or a cell. Its value of 0 indicates a perfect cell, while the value of 1 indicates a degenerate (nearly colinear) cell. Generally, in all generated meshes the greatest number of elements had skewness value below 0.05. However, the elongated rectangles forming the first few layers of the boundary layer slightly ruin these statistics. That is why averaged

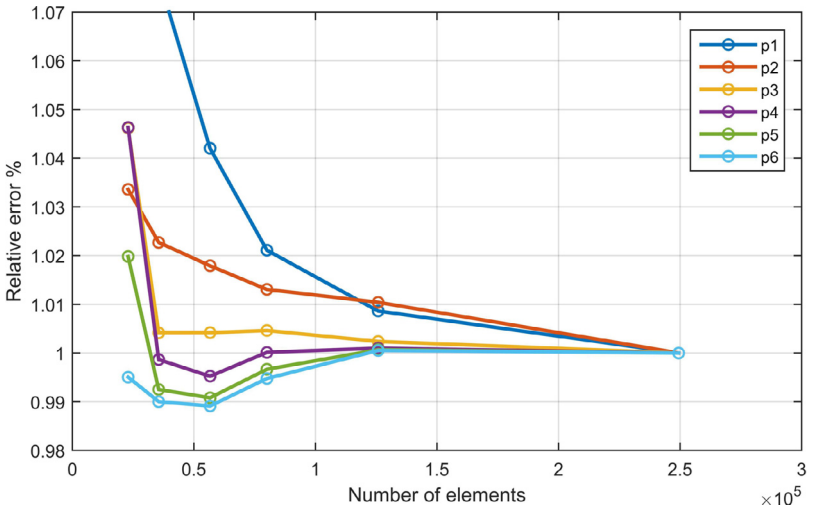

Fig. 7. Relative errors of the Mach number values at six different reference points (p1 - p6) for different computational meshes.

Table 4
Experimentally measured data and ER.

Spindle position, %	m_p [kg/s]	m_s [kg/s]	ER
10	0.10650 ± 0.00106	0.06250 ± 0.00062	0.58685 ± 0.01057
20	0.11010 ± 0.00110	0.06940 ± 0.00069	0.63033 ± 0.01076
30	0.11370 ± 0.00114	0.0750 ± 0.00075	0.65963 ± 0.01090
40	0.11790 ± 0.00118	0.08190 ± 0.00082	0.69465 ± 0.01110
50	0.12290 ± 0.00123	0.08750 ± 0.00087	0.71196 ± 0.01121
60	0.12750 ± 0.00127	0.09440 ± 0.00094	0.74039 ± 0.01140

values of the skewness factor seem somewhat higher (Table 3). The orthogonal quality metric in 2D meshes estimates the relation of edge normal vector to the corresponding vector connecting the centroids of the current and adjacent faces. Its range is again 0–1, where 0 is worst, and a value of 1 is best. Mesh metrics of exemplary generated meshes (spindle at 40%) is presented in Table 3.

As previously stated, the values of Mach number at six different chosen points were used for mesh independency study. The relative errors of obtained values are presented in Fig. 7. Moreover, Mach number distribution along three different cross-sections and the axis at M6, M5 and M3 computational grids are shown in Fig. 8a and 8b, respectively.

Mesh properties of the M5 grid can be considered satisfactory (relative error is approximately 1%) and were used for the remainder of the study. All following meshes are 2-D, hybrid unstructured with 20 prismatic layers on the wall surfaces resulting in dimensionless wall distance $y+ < 5$. They are all appropriate for axisymmetric simulations of the flow (half-model is used) and contain approximately 130 thousand cells (depending on the nozzle geometry). An example of a part of the created mesh, around the variable area nozzle is presented in Fig. 9.

6. Results and discussion

The scope of the research is to make an appropriate performance evaluation of a supersonic ejector with the novel, designed variable area nozzle and to confirm advantages of applying it in further studies, especially in the field of ejector performance optimization. Experimentally measured data and ER with uncertainties are shown in Table 4, whereas comparison of analytical and numerical results to the obtained experimental data is presented in Fig. 10 and Table 5.

Relative errors of the numerical model predictions of ER vary with geometry between 12% for 10% spindle position and 0.96% for 40% spindle position, whereas the corresponding 1-D model prediction errors are between 25% and 2%. Furthermore, a similar evaluation is made for secondary and primary mass flow rates. It should be emphasized that 1-D model results for a mass flow rate of the motive fluid showed negligible errors in comparison with CFD results. Conversely, the upper errors of secondary stream mass flow rate are around 25% and 20% for 10% spindle position for analytical and numerical predictions, respectively.

Possible reasons of the overestimated influence of the spindle position in the 1-D model compared with experiments could be due to the assumption of the ideal gas mixture, negligence of high friction loss across the spindle and oblique shock waves. In the case of the CFD approach, the assumption of single phase flow is the probable cause of slightly higher, but still acceptable, model relative errors. Since satisfactory correspondence between different sets of results is achieved, various additional numerical analyses were performed.

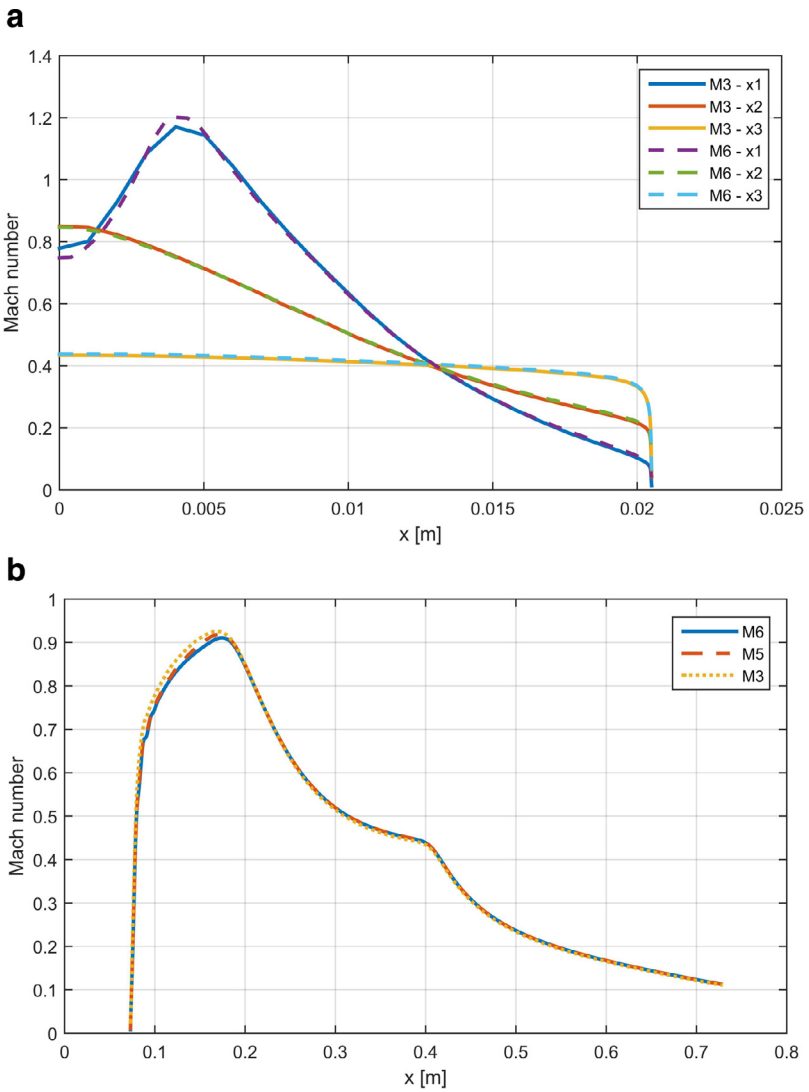

Fig. 8. Mach number distribution along three different cross-sections (a) and the axis (b) at different computational grids.

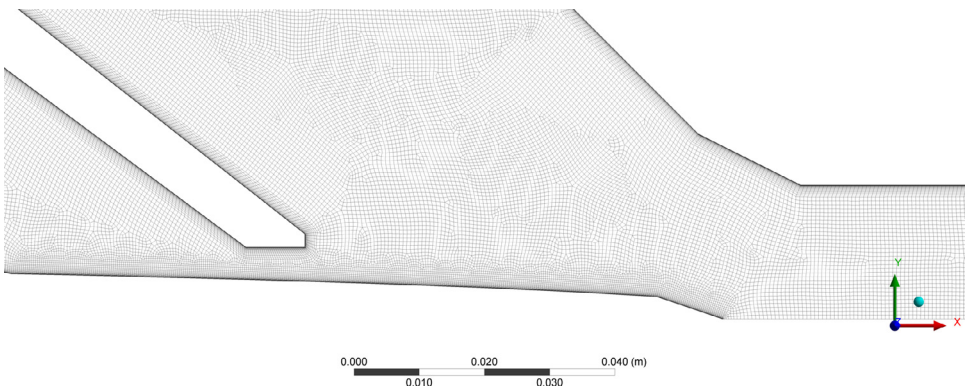

Fig. 9. Mesh density in the nozzle region.

Table 5
Relative errors of ER obtained by different models at outlet gauge pressure $p_{out} = 30$ kPa.

Spindle position, %	1-D model						CFD - Fluent					
	m_p [kg/s]	m_s [kg/s]	ER	Relative error m_p, %	Relative error m_s, %	Relative error ER, %	m_p [kg/s]	m_s [kg/s]	ER	Relative error m_p, %	Relative error m_s, %	Relative error ER, %
10	0.1070	0.0469	0.44	0.50	24.96	25.21	0.0958	0.0495	0.52	10.03	20.81	11.97
20	0.1109	0.0590	0.53	0.72	15.04	15.65	0.0993	0.0572	0.58	9.84	17.64	8.66
30	0.1151	0.0708	0.62	1.21	5.60	6.75	0.1029	0.0643	0.62	9.47	14.31	5.36
40	0.1193	0.0813	0.68	1.22	0.79	2.05	0.1067	0.0735	0.69	9.50	10.36	0.96
50	0.1237	0.0913	0.74	0.66	4.34	3.65	0.1105	0.0835	0.76	10.11	4.56	6.17
60	0.1281	0.1004	0.78	0.45	6.31	5.86	0.1145	0.0911	0.80	10.24	3.54	7.44
Averaged				0.79	9.51	9.86				9.86	11.87	6.76

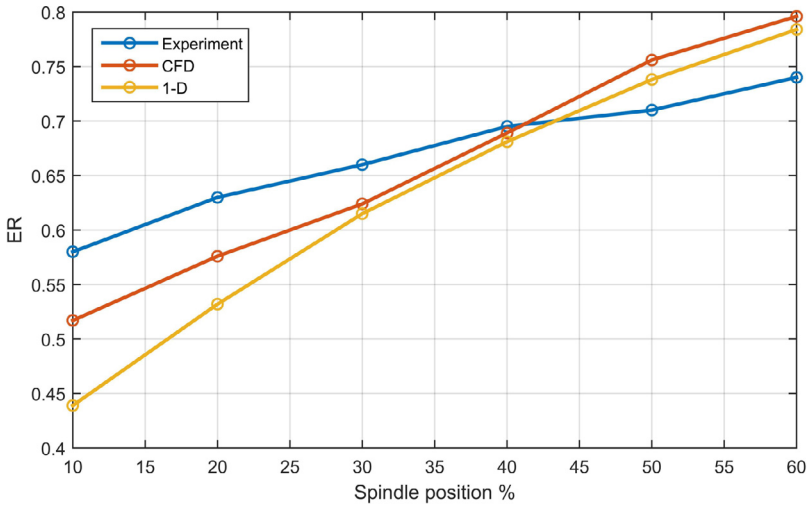

Fig. 10. Comparison of experimental, analytical and numerical data at outlet gauge pressure $p_{out} = 30$ kPa.

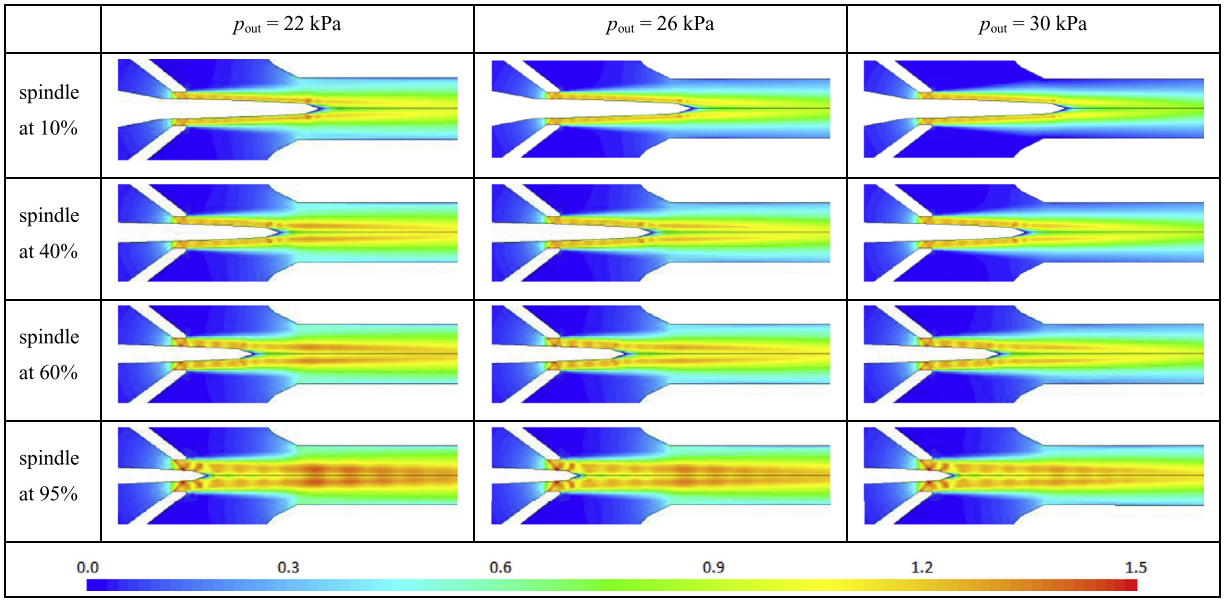

Fig. 11. Mach number contours (in the nozzle region and parts of suction and mixing chambers) at different spindle locations (10%, 40%, 60% and 95%) and different outlet gauge pressures ($p_{out} = 22$ kPa, 26 kPa and 30 kPa).

The spindle position primarily defines the nozzle geometry (cross-section area and shape). Therefore, the flow through the nozzle can only be changed (i.e. controlled) by the translation of the spindle in the axial direction. This statement can be confirmed by analyzing the rows of Fig. 11 and Table 5.

In the 1-D model, it is assumed that the suction chamber pressure is always equal to secondary flow inlet pressure, so the velocity of the primary fluid at the nozzle outlet is independent of mixture outlet pressure and Mach number is equal to 1.214. Mach numbers at the nozzle outlet for different spindle positions, obtained by CFD analysis, are presented in Table 6. Although nozzle outlet Mach numbers are in accordance with 1-D calculated values, strong and weak shock waves are distributed along spindle edges in the suction chamber. Compression ratio (CR) contours for different spindle positions at constant outlet pressure are presented in Fig. 12. It can be observed that oblique shock waves are the strongest at the top of the spindle. Nonetheless, these disturbances do not significantly affect overall ejector performances, concerning ER and CR.

Independently from the imposed values of the outlet pressure (22 kPa, 26 kPa or 30 kPa) the flow pattern inside the nozzle remains almost the same (Fig. 11). The changes become noticeable near the tip of the spindle where the entrainment of the secondary flow only just begins. On the other hand, the outlet pressure value significantly influences the flow in the mixing chamber and the diffuser. The decrease in the outlet pressure noticeably increases both the supersonic zone as well

Table 6
Values of Mach number at the nozzle outlet for outlet gauge pressure $p_{out} = 30$ kPa.

Spindle position (%)	M_1
10.00	1.2111
20.00	1.2160
30.00	1.2192
40.00	1.2245
50.00	1.2307
60.00	1.2384
95.00	1.2731

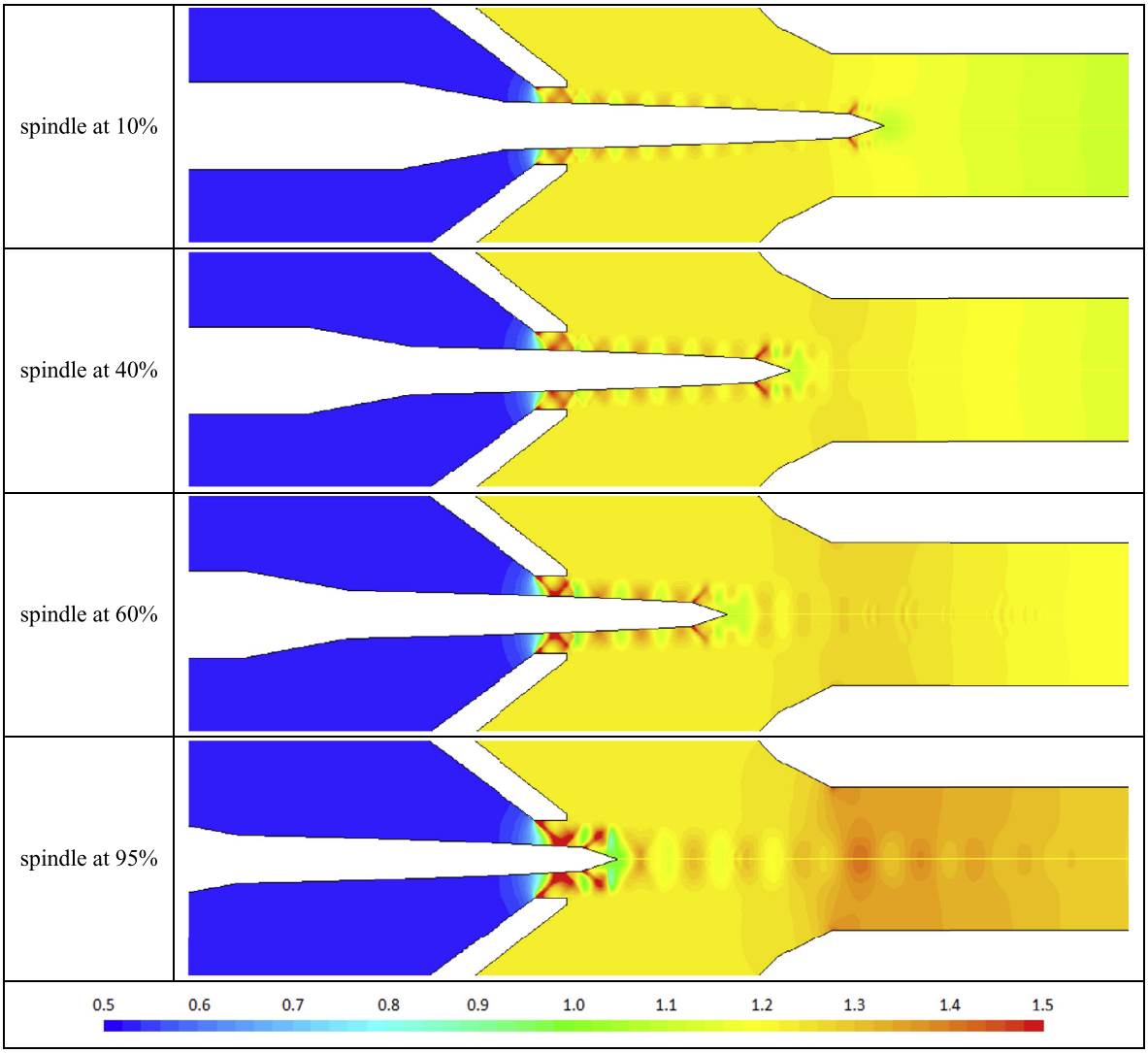

Fig. 12. CR contours around and behind the spindle for different spindle locations (10%, 40%, 60% and 95%) and constant outlet pressure $p_{out} = 30$ kPa.

as the ensuing zone of higher flow speeds resulting in slower mixing and more non-uniform flow field. Other consequences of the outlet pressure drop down regarding the mixing layer are that in the mixing chamber it is closer to the axis while it is less inclined from the axis (i.e. more horizontal) in the diffuser which is shown in Figs. 13 and 14.

A similar effect can be achieved by translating the spindle while keeping the constant value of the outlet pressure (Figs. 11, 13 and 14); however, oblique shock waves are more dominant in the cases where the top of the spindle is positioned closer to the nozzle outlet. Not every combination of the spindle position and outlet pressure produces satisfactory

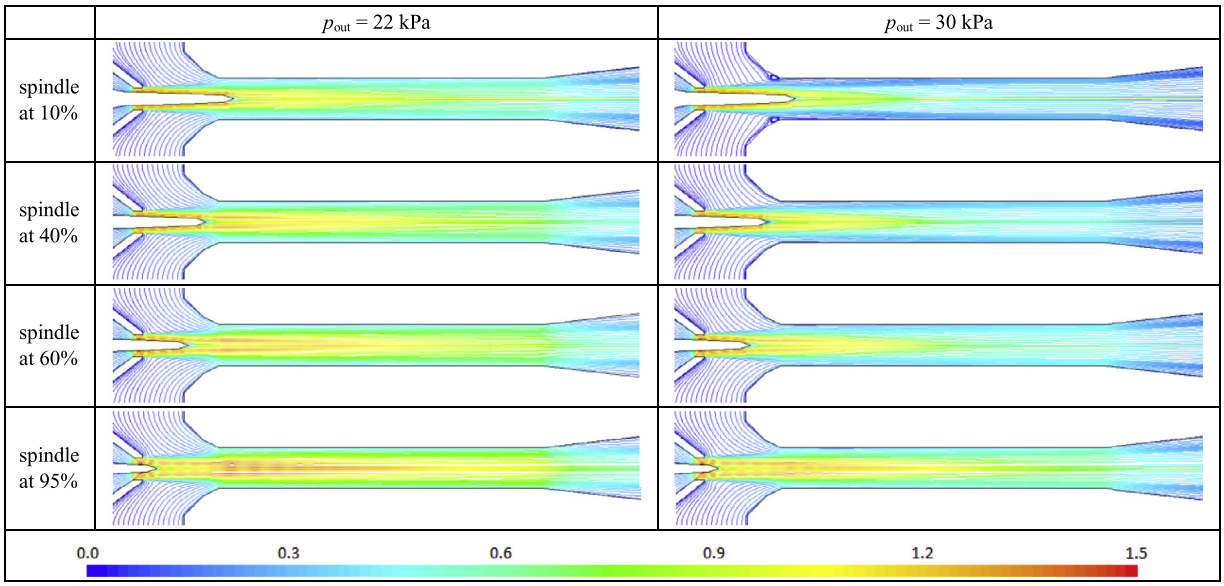

Fig. 13. Streamlines originating from the two inlet surfaces colored by Mach number values at different spindle locations (10%, 40%, 60% and 95%) and different outlet gauge pressures (p_{out} = 22 kPa and 30 kPa).

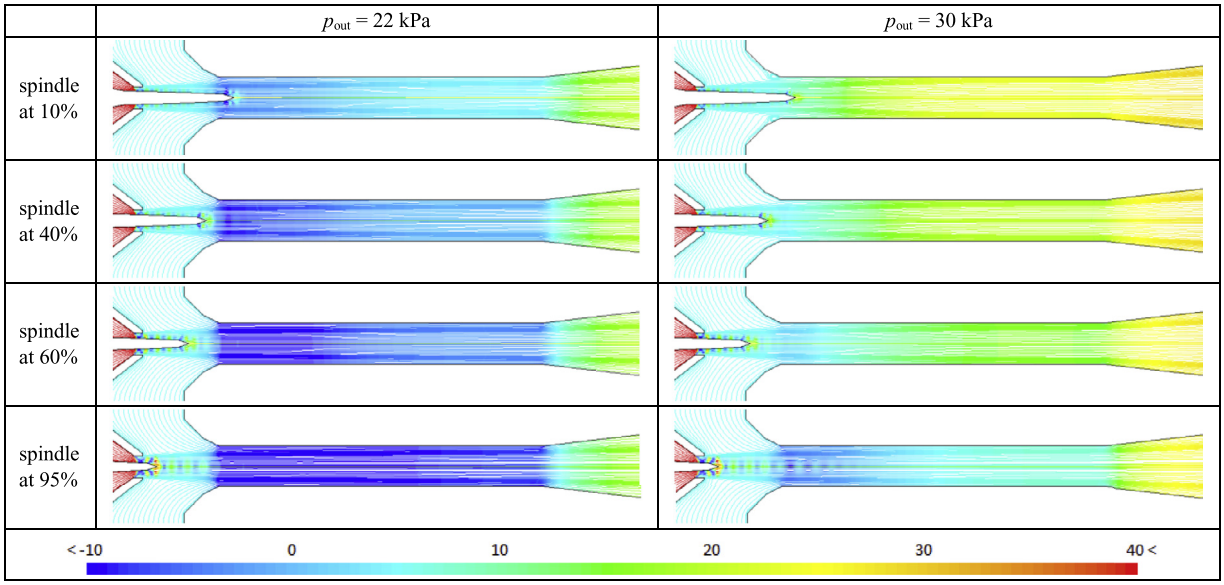

Fig. 14. Streamlines originating from the two inlet surfaces colored by gauge pressure values [kPa] at different spindle locations (10%, 40%, 60% and 95%) and different outlet gauge pressures (p_{out} = 22 kPa and 30 kPa).

results. From Figs. 13 and 14 it can be seen that insufficient pressure difference together with small nozzle area can introduce zones of recirculating flow.

Fig. 15 illustrates Mach number distributions for different geometries at a constant value of outlet pressure. The occurrence of velocity sudden increase and progressive reduction in the mixing chamber, as well as the second velocity decrease in the diffuser, are well illustrated. As expected, lower values of spindle position produce smaller velocities. For the spindle located at 10%, the flow in the mixing chamber is purely subsonic with only a small sonic zone appearing in the nozzle region. When the spindle is translated backwards, the sonic zone slowly increases, so that Mach number reaches maximal values of around 1.2–1.3 at the axis. At higher spindle positions (60% and 95%) shock wave existence and interaction become apparent (oscillations of Mach number profile along the axis indicate the existence of a row of oblique shock waves). In addition, for higher spindle positions, strong shockwaves move forwards along the axis of the mixing chamber, whereas the velocity profile is more uniformly distributed at the end of the mixing chamber for lower spindle position.

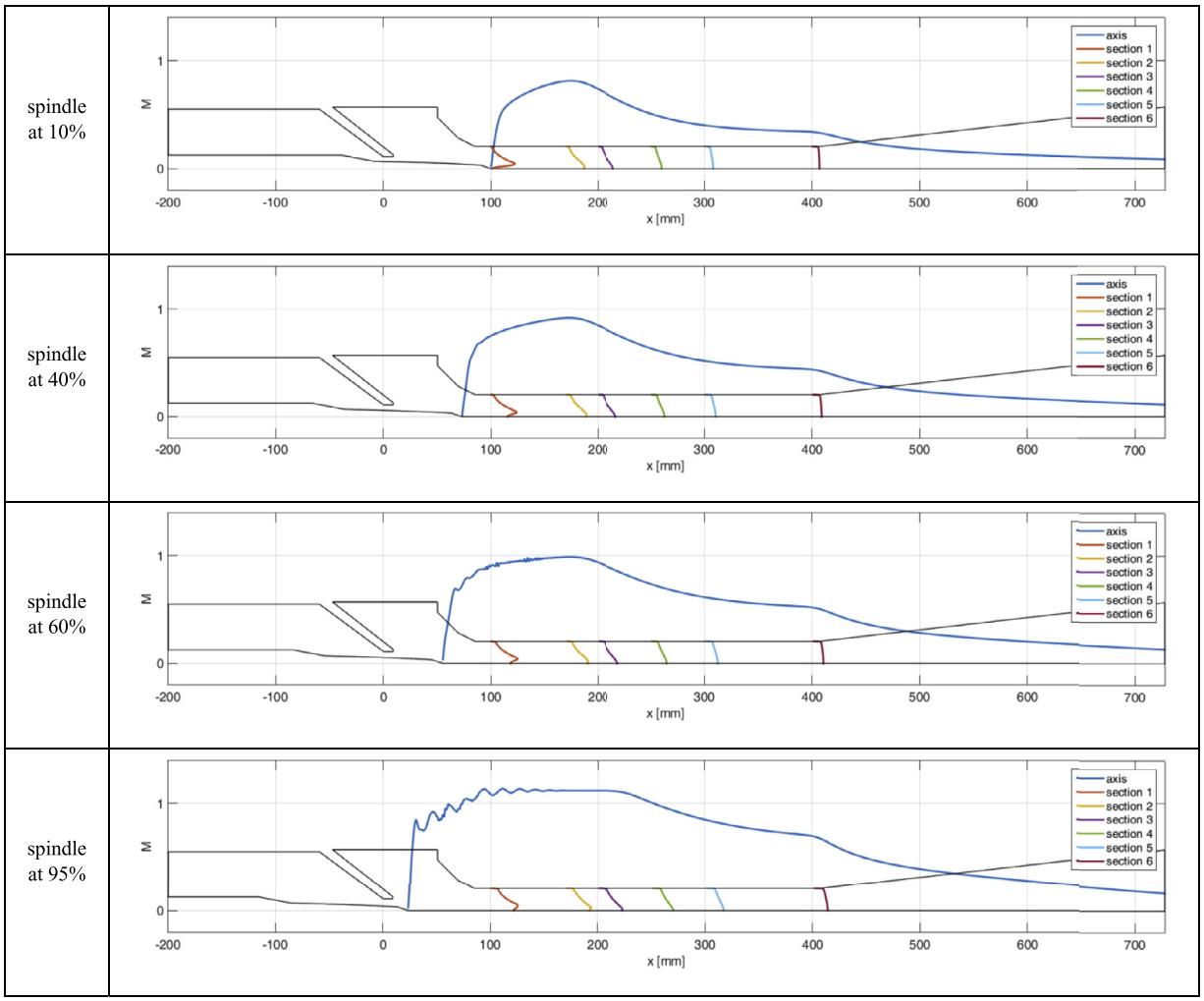

Fig. 15. Mach number profiles along the axis and six cross-sections at different spindle locations (10%, 40%, 60% and 95%) and constant outlet pressure $p_{out} = 30$ kPa).

Mixing of the two fluid streams is illustrated by Figs. 13–15. Although the streamlines from the two sources (inlet surfaces) are uninterrupted, the momentum exchange is apparent. By analyzing Mach number and pressure distributions in the mixing chamber, it can be concluded that the distributions are continuous and differentiable. Maximum velocity is achieved when the accelerated streams are leaving the nozzle to unite in the central part of the mixing chamber. With the decrease in the outlet pressure velocity increases while the merging point moves further away from the spindle tip.

By varying both the outlet pressure and spindle position, a complete map of variable nozzle ejector characteristics can be formed. The outlet pressure reduction leads to an ER increase, for all spindle positions. However, the gradient of the change is the greatest for 10%, and the smallest for 95%, spindle position (Fig. 16a and 16b). Now, it is more evident that the spindle position becomes increasingly important at higher p_{out}, where differences in ER become significant. One of the reasons for this is a possible choking condition in the mixing chamber due to the large mass flow rate of the secondary flow for small values of outlet pressure.

The main disadvantage of an ejector with this kind of variable area nozzle is the possibility of choking, especially in the case when the spindle is moved forward, so that entrance area of the mixing chamber is decreased by the cross-sectional area of the spindle. Unless the mixing chamber cross section area is also changeable, it is not possible to design such a variable nozzle area ejector in which translation of the spindle changes the mass flow rate of the primary flow as well as producing choking in the mixing chamber while preserving ER and CR within narrow limits. This is the reason why the unchoked flow of the secondary stream is not defined as off-design in this particular situation. Other disadvantages are connected with the high friction loss at the nozzle, due to the length of the spindle and high velocities of primary flow at the nozzle outlet.

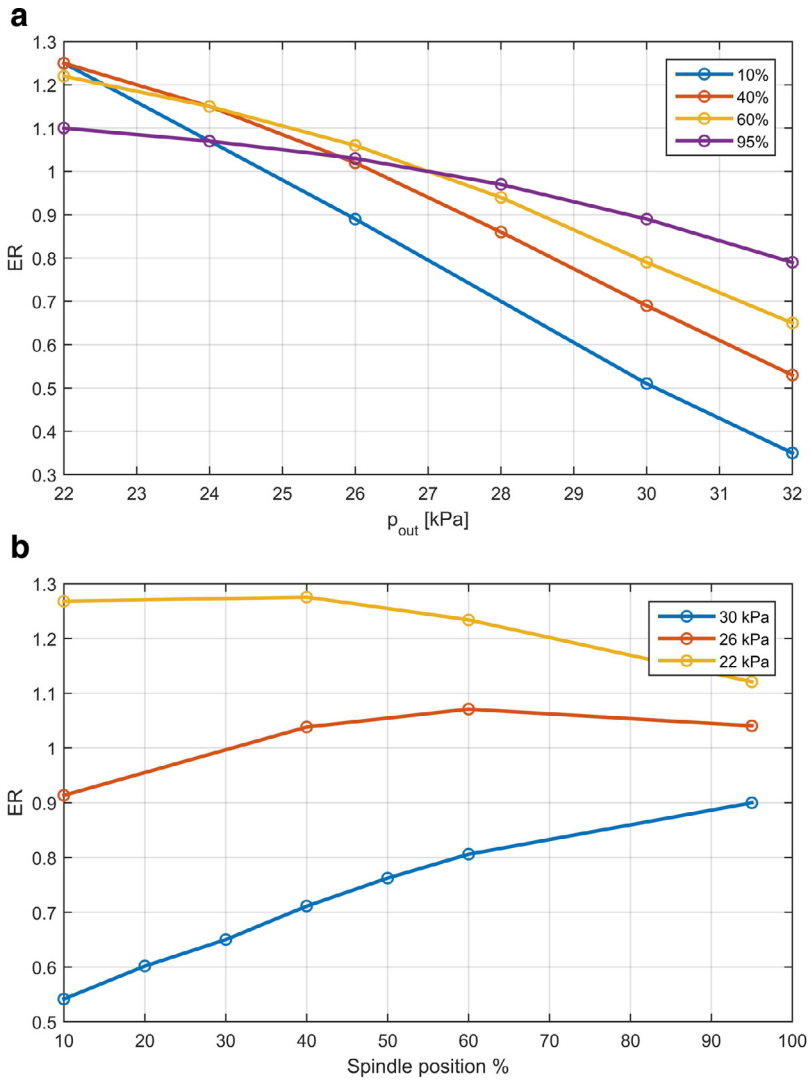

Fig. 16. ER change: with outlet pressure p_{out} and constant spindle position (a); with spindle position and constant outlet gauge pressure p_{out} (b).

7. Conclusion

In this paper, a novel method for the design of a variable area nozzle has been presented and validation of its usage in ejector performance optimization was carried out by experimental, numerical and analytic approaches. The ejector with a variable area nozzle using natural gas as the motive fluid and waste gas as the secondary fluid proved to be very efficient in holding the values of ER and CR in narrow limits, while varying mass flow rates of the primary and secondary fluid. The k-ω SST model was used for closure of compressible momentum equations in CFD model. Both numerical and analytic models showed satisfactory prediction performance in comparison with the experimental data. Four key findings are emphasized as follows:

1. The design of the nozzle was based on 1-D isentropic modeling of a convergent-divergent nozzle. The nozzle is constructed using a spindle and cylinder. Moving the spindle along the axis of the nozzle changes the cross-section area of the throat and consequently changes the mass flow rate. The spindle was designed to maintain a constant nozzle area ratio to prevent irreversibility and consequent reduction in momentum.
2. The enormous disadvantage of this nozzle construction is high friction loss due to the length of the spindle. For that reason, a compromise between the length of the spindle and the operating conditions (ER and CR limits) has to be made, to successfully construct a supersonic ejector.

3. The un-choked flow of the secondary stream is not considered as off-design since the ejector has to maintain ER and CR in narrow limits while changing the mass flow rate of the primary fluid. Possible improvements to this kind of ejector might involve varying the cross-section area of the mixing chamber.
4. The CFD model of the ejector confirmed that although supersonic flow zones may appear at the nozzle outlet, the disturbances in the form of a series of shock waves have little effect on total pressure drop. Furthermore, experimental and numerical data showed that the ejector with variable area nozzle can be used efficiently for a wide range of the flow parameters. Further investigation of ejectors of this type, their possible applications and optimal operation in industry, can be the subject of future study.

Acknowledgment

The research work is performed as a part of Technological Development Projects nos. 35035, 35046, 35031, 35011, 174002 funded by the Ministry of Science, Education and Technological Development of the Republic of Serbia. The authors would also like to express gratitude to member companies which were involved in the construction of installation at factory “FSK Elemir” for helping us to measure the data presented in this article.

References

[1] A. Foley, A.G. Olabi, Renewable Energy Technology developments, Trends and Policy Implications That Can Underpin the Drive For Global Climate Change, Elsevier, 2017.
[2] P. Milanović, B. Jaćimović, S. Genić, The influence of heat exchanger performances on the design of indirect geothermal heating system, Energy Build. 36 (2004) 9–14.
[3] M. Stamenić, B. Jaćimović, S. Genić, G. Jankes, T. Simonović, N. Tanasić, Results of experimental research on parameters that determine stable operating limits of ceramic burner with packed bed of uniform spheres for combustion of low calorific gaseous fuels, in: Proceedings of the 3rd International Symposium on Environmental Friendly Energies and Applications (EFEA), IEEE, 2014, pp. 1–5.
[4] F. Zhou, T. Xia, X. Wang, Y. Zhang, Y. Sun, J. Liu, Recent developments in coal mine methane extraction and utilization in China: a review, J. Nat. Gas Sci. Eng. 31 (2016) 437–458.
[5] C. Friesenhan, I. Agirre, L. Eltrop, P.L. Arias, Streamlined life cycle analysis for assessing energy and exergy performance as well as impact on the climate for landfill gas utilization technologies, Appl. Energy 185 (2017) 805–813.
[6] B. Huang, J. Chang, C. Wang, V. Petrenko, A 1-D analysis of ejector performance, Int. J. Refrig. 22 (1999) 354–364.
[7] C. Liao, Gas Ejector Modeling For Design and Analysis, Texas A&M University, 2008.
[8] S. Elbel, N. Lawrence, Review of recent developments in advanced ejector technology, Int. J. Refrig. 62 (2016) 1–18.
[9] Y.M. Antonio, C. Périlhon, G. Descombes, C. Chacoux, Thermodynamic modelling of an ejector with compressible flow by a one-dimensional approach, Entropy-Switz 14 (2012) 599–613.
[10] A. Hemidi, F. Henry, S. Leclaire, J.-M. Seynhaeve, Y. Bartosiewicz, CFD analysis of a supersonic air ejector. Part I: experimental validation of single-phase and two-phase operation, Appl. Therm. Eng. 29 (2009) 1523–1531.
[11] S. Croquer, S. Poncet, N. Galanis, Comparison of ejector predicted performance by thermodynamic and CFD models, Int. J. Refrig. 68 (2016) 28–36.
[12] S. Croquer, S. Poncet, Z. Aidoun, Turbulence modeling of a single-phase R134a supersonic ejector. Part 1: numerical benchmark, Int. J. Refrig. 61 (2016) 140–152.
[13] G. Besagni, F. Inzoli, Computational fluid-dynamics modeling of supersonic ejectors: screening of turbulence modeling approaches, Appl. Therm. Eng. 117 (2017) 122–144.
[14] A. Balabel, A. Hegab, M. Nasr, S.M. El-Behery, Assessment of turbulence modeling for gas flow in two-dimensional convergent–divergent rocket nozzle, Appl. Math. Model. 35 (2011) 3408–3422.
[15] T. Thongtip, S. Aphornratana, An experimental analysis of the impact of primary nozzle geometries on the ejector performance used in R141b ejector refrigerator, Appl. Therm. Eng. 110 (2017) 89–101.
[16] S. Varga, A.C. Oliveira, X. Ma, S.A. Omer, W. Zhang, S.B. Riffat, Experimental and numerical analysis of a variable area ratio steam ejector, Int. J. Refrig. 34 (2011) 1668–1675.
[17] C. Li, Y. Li, W. Cai, Y. Hu, H. Chen, J. Yan, Analysis on performance characteristics of ejector with variable area-ratio for multi-evaporator refrigeration system based on experimental data, Appl. Therm. Eng. 68 (2014) 125–132.
[18] C. Li, J. Yan, Y. Li, W. Cai, C. Lin, H. Chen, Experimental study on a multi-evaporator refrigeration system with variable area ratio ejector, Appl. Therm. Eng. 102 (2016) 196–203.
[19] M. Dennis, T. Cochrane, A. Marina, A prescription for primary nozzle diameters for solar driven ejectors, Solar Energy 115 (2015) 405–412.
[20] D. Lelea, A.E. Cioabla, The viscous dissipation effect on heat transfer and fluid flow in micro-tubes, Int. Commun. Heat Mass 37 (2010) 1208–1214.
[21] P.R. Pereira, S. Varga, J. Soares, A.C. Oliveira, A.M. Lopes, F.G. de Almeida, J.F. Carneiro, Experimental results with a variable geometry ejector using R600a as working fluid, Int. J. Refrig. 46 (2014) 77–85.
[22] S. Varga, A.C. Oliveira, A. Palmero-Marrero, J. Vrba, Preliminary experimental results with a solar driven ejector air conditioner in Portugal, Renew. Energ. 109 (2017) 83–92.
[23] P.H. Oosthuizen, W.E. Carscallen, Introduction to Compressible Fluid Flow, CRC Press, 2013.
[24] F. Kong, H. Kim, Analytical and computational studies on the performance of a two-stage ejector–diffuser system, Int. J. Heat Mass Transf. 85 (2015) 71–87.
[25] A. Bouhanguel, P. Desevaux, E. Gavignet, Flow visualization in supersonic ejectors using laser tomography techniques, Int. J. Refrig. 34 (2011) 1633–1640.
[26] E.J. Sokolov, Flow machines (in Russian), vol. 3, Moscow Energoatomizdat, 1989.
[27] Fluent, A.N.S.Y.S. “14.0 User’s Manual.” ANSYS Inc., Canonsburg, PA (2011).